Effect of shear stresses on fibre direction tensile failure using a new simple and reliable test method with thin plies

Jalalvand, Meisam; Fotouhi, Mohammad; Wisnom, Michael R.

Important note
To cite this publication, please use the final published version (if applicable).
Please check the document version above.

Effect of shear stresses on fibre direction tensile failure using a new simple and reliable test method with thin plies

Meisam Jalalvand [a],[*], Mohammad Fotouhi [b], Michael R. Wisnom [c]

[a] *Engineering Materials, School of Engineering, University of Southampton, UK*
[b] *MICROLAB, Faculty of Civil Engineering and Geosciences, Delft University of Technology, Netherlands*
[c] *Bristol Composites Institute, University of Bristol, UK*

A B S T R A C T

A new method of creating in-plane combined tension-shear stress states using only tensile loading is proposed. Thin-ply angle-ply carbon/epoxy laminates are sandwiched between unidirectional glass layers to eliminate any stress concentration around the samples ends and gripping zone. Use of the thin plies successfully suppresses early occurrence of other modes of failure i.e. matrix cracking and free-edge delamination, so the first mode of failure is fibre failure in the angle-ply carbon sub-laminate. Compared with other methods of creating combined tension-shear stresses, the proposed technique has a simpler geometry, is significantly easier and cheaper to manufacture and test. Therefore, it provides more repeatable low-scatter experimental results.

The obtained experimental results showed that the presence of in-plane shear stresses did not have a significant impact on the tensile fibre-direction failure strain of the tested carbon/epoxy laminate, suggesting that even at high shear stresses, the longitudinal tensile strength of the carbon/epoxy laminate is not significantly reduced.

1. Introduction

The failure process of Fibre Reinforced Polymer (FRP) Composite materials is complicated to understand and predict. Composites demonstrate direction dependency in the elastic regime and have many failure modes such as fibre failure, matrix cracking, delamination between the layers and fibre/matrix interfacial debonding. There are numerous material and geometrical parameters that affect the failure process and trigger different modes of failure that are typically not considered in design procedures and are still under further research. For instance, the ply thickness, total laminate thickness, fibre volume fraction, fibre misalignment and size effect are some of those that add to this complexity. On top of these, the failure process of composites is usually catastrophic which makes their testing and precise capture of the experimental results more challenging compared to more ductile materials.

This complicated nature of composites has led to development of several different theories and approaches to predict failure that do not typically match each other. This disagreement and abundance of approaches to predict failure caused concerns in the 1990 s as it proved to be difficult for designers to pick the '*right*' failure criterion. Extensive collective efforts such as World-Wide Failure Exercise (WWFE) between

1994 and 2004 aimed to sift through the best available theories and showcase the success rate of the available theories. However, one of the most important conclusions made through such activities was the lack of precise experimental results, as quoted in [1]: "Not entirely unexpectedly, as the [WWF] exercise proceeded, it became clear that the experimental data was judged to be inadequate in a number of critical areas… As one probed theories more deeply, the experimental evidence became insufficient or unreliable to draw further conclusions…Definitive experimental data is hard to come by in the field of composite materials, and that a degree of greyness, and scepticism, is always present…".

The challenge of having reliable and precise experimental results remains a major challenge to date. Commonly agreed measurement techniques are limited to a few mechanical properties and for more advanced properties or complex loading cases, there are no standards. More importantly, following standards does not necessarily lead to suppression of undesired failure modes in the experimental data. For instance, standards such as ISO 527–5 [2], ASTM D5083–10 [3] and ASTM D3039/D3039M–08 [4] for measuring longitudinal strength of FRP composites, probably the most basic mechanical property of composites, introduce stress concentrations at the end-tabs and therefore underestimate the strength of Uni-Directional (UD) composites. This has been demonstrated in more details by Czél et al [5]. In the same paper,

---

* Corresponding author.
  E-mail address: m.jalalvand@soton.ac.uk (M. Jalalvand).

the authors proposed a new way of eliminating stress concentrations and measuring the failure strain reliably by using a translucent continuous end-tab configuration, making the failure point visually detectable and consistently away from the grips [5]. This technique is not suitable for ductile materials but suits the properties and failure process of FRP composites and the authors believe similar techniques, especially designed for composites rather than being adapted from ductile homogeneous materials, are necessary to build reliable experimental data.

In this paper, we propose a new method to measure the longitudinal (fibre direction) tensile failure strain of UD carbon/epoxy layers ($\hat{\varepsilon}_1$) in the presence of in-plane shear strain ($\hat{\gamma}_{12}$). These measurements are directly related to their stress counterparts and hence to the longitudinal failure stress ($\hat{\sigma}_1$) and in-plane shear failure stress of a UD laminate ($\hat{\tau}_{12}$). The hat symbol, $\hat{}$, indicates the variable underneath it is at the failure point. Also, please note that, variable $\hat{\sigma}_1$ is used deliberately instead of X_T since the stress state is not uniaxial, and it includes shear stress. So, the longitudinal failure stress $\hat{\sigma}_1$ is not necessarily equal to X_T. The longitudinal-shear combined stress is one of the combined stress states where the predictions of several different failure theories do not match. Fig. 1 (a) indicates the comparison of different theories against each other and against the experimental results used in the WWFE to find the most accurate one. Clearly, the difference between the theories increases at high values of shear stress. Some of the theories predict low longitudinal failure stress in the presence of shear stress but there are other theories in which, the longitudinal failure stress is not affected by shear stress at all. More importantly, and despite all the efforts of the

WWFE organisers to find the most reliable experimental results, the scatter in the experimental results is high which limits its use as a benchmark to judge between the different theories. Please note that subscript 123 is in the local materials coordinate system with 1 referring to the fibre direction, 2 the in-plane transverse direction and 3 the through-thickness. The subscripts used for global loading directions are xyz with x indicating the loading direction. As an example, τ_{12} is the shear stress in the local material coordinate system with 1 along the fibres and 2 transverse to the fibre which is different from τ_{xy}, the shear stress in the global coordinate system with x along the loading direction and y along the width of the sample. For instance, the τ_{xy} shear stress component approaches zero at the free-edges due to the existence of a free surface however, τ_{12} does not become zero as the 12 coordinate system is not aligned with the free surface at the edges.

The common methods to achieve biaxial states of stress are: 1) axial loading together with internal pressure or torsion on tubular specimens, 2) flat cruciform specimens with biaxial loading applied to the arms and 3) plate specimens under biaxial bending moments [6]. Among these options, the tubular specimen is known to be theoretically the most versatile one. All three in-plane stresses can be applied independently from each other and the free-edge effect is not present. Axial stresses are applied by axial tension or compression, hoop stresses by inner or outer pressure, and shear stress by torsion [7]. However, the practical aspect of manufacturing tubular samples with a section suitable for smoothly applying the load is far from simple. The typical manufacturing process of such tubes is filament winding which requires relatively capital-
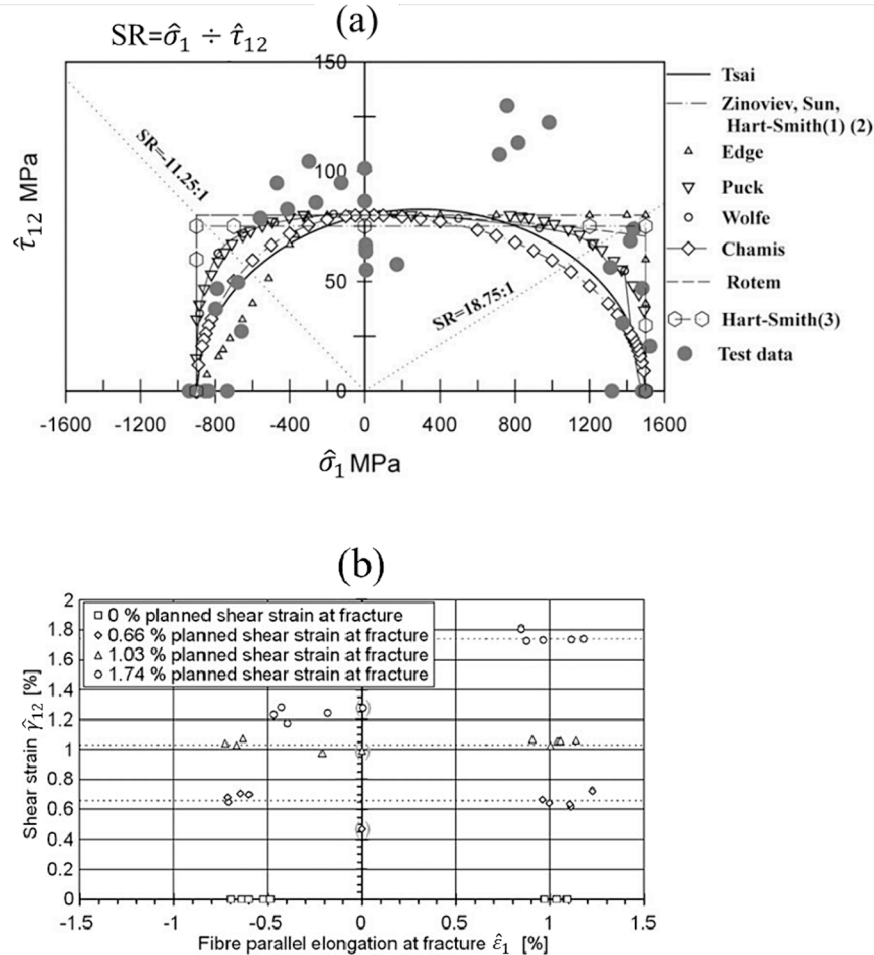

Fig. 1. (a) Comparison between the predicted and measured biaxial longitudinal/shear failure stresses for 0° lamina made of CFRP material T300/914C -Test Case No 2 in the WWFE adapted from [1], (b) Longitudinal failure strain ($\hat{\varepsilon}_1$) at different applied in-plane shear strain ($\hat{\gamma}_{12}$) of T300/ Araldite LY556/HY917/DY070 epoxy adapted from [9].

intensive facilities. The major source of stress inhomogeneities is the collets. When tubes without reinforced end sections are used, failure normally occurs near the grips. The most common design for the reduction of stress concentrations is thickened end sections which makes the manufacturing process more complicated and still introduces stress concentrations [7]. Also, filament winding can lead to fibre volume fraction or manufacturing defects different from standard prepreg manufacturing and therefore the values may not be directly comparable.

Creating controlled tension-shear coupling to achieve failure of the FRP under combined longitudinal normal and shear stress is a challenge. The experimental results in Fig. 1 (a) were achieved from specimens in the form of axially wound tubes made from T300/BSL914C carbon/ epoxy prepreg [8]. The tubes were tested under combined axial tension or compression and torsion. All the tubes were end reinforced and grips were used to transmit the torque to the tubes.

In a similar study, two different tubular specimens with fibres in the longitudinal and circumferential directions were manufactured and then were loaded under axial tension plus torsion and internal pressure respectively [9]. The material tested was T300/Araldite LY556/HY917/ DY070 epoxy which is the same fibre as [8]. The results from the tubes with fibres in the circumferential direction showed a wide scatter and were not reported in the paper. The results for the tube with fibres parallel to the axis of the tube in the form of in-plane shear strain at failure ($\widehat{\gamma}_{12}$) versus longitudinal failure strain ($\widehat{\varepsilon}_1$) are shown in Fig. 1 (b). The authors concluded that application of shear stress does not change the carbon fibre failure strain.

The experimental results presented in [9] have less scatter than that in [8] however, the values of failure stress/strain at no in-plane shear strain (the experimental markers in Fig. 1 (a and b) on the horizontal axis at $\widehat{\gamma}_{12} = 0$) in both [8,9] are significantly lower than the values of T300 composite longitudinal strength of 1820 MPa and failure strain of 1.26 % [10]. The average strength of the material under pure axial load in [8] is 1434 MPa which is 22 % lower than 1820 MPa reported in the data sheet. The 1.0 % average pure longitudinal failure strain from Fig. 1 (a) is also 21 % lower than the T300 composite failure strain reported in the data sheet. It is worth mentioning that ASTM D3039 [11] was used as the test method to measure the strength of the T300 composite in the data sheet [10], and in a previously published paper [5], the authors showed that such standards underestimate the real strength of composite materials as the end-tabs introduce stress concentrations and the specimens usually fail at the end-tabs. So the difference between the results reported in [8,9] and the true strength of T300 composites could be even more than the 21 % and 22 % mentioned above.

The aim of this paper is to propose a new way of generating combined in-plane tension-shear stress state in a flat coupon that doesn't suffer from end-tab stress concentrations, early matrix transverse cracking or free-edge delamination. Combined tension-shear stress states are achieved by applying tension on angle-ply carbon laminates. Thin-plies are used in the manufacture of the angle-ply CFRP laminate so early matrix transverse cracking as well as free-edge delamination are suppressed [12]. Finally, the angle-ply carbon laminates are embedded between unidirectional glass/epoxy layers to eliminate the stress concentration at the end-tabs as shown in the authors previous work [5]. The strains are measured directly and therefore, the experimental results are based on the measured in-plane longitudinal (ε_1) and shear (γ_{12}) strains. The obtained results are compared against the failure strain of the material under pure tension. The geometry, manufacture and testing of the proposed samples are significantly easier compared against the tubular samples under uniaxial tension plus torsion and the obtained experimental data have far less scatter when compared against those from tubular specimens in [8,9].

2. Concept

The main aim is to achieve longitudinal fibre failure in a unidirectional lamina under combined in-plane tension-shear stress states. The stress in each ply of a $[\pm\theta]_s$ angle-ply laminate ($\theta < 45°$) under pure tension is mainly a combination of both tension along the fibres, σ_1, and shear stress, τ_{12}. It will be shown that the transverse stress perpendicular to the fibre direction is small and can be neglected. The longitudinal stresses in all the $+\theta$ layers are the same as those in the $-\theta$ layers and the shear stresses are also the same but with opposite signs. Through thickness stresses away from the free-edges are negligible. Therefore, failure of a $[\pm\theta]_s$ angle-ply laminate under pure tension can potentially occur due to longitudinal failure under combined tension-shear stress without the influence of other stress components. However, it is important to remember that other failure modes e.g. free-edge delamination, matrix cracking or failure at the end-tabs can occur before the longitudinal failure of the plies. In such cases, the failure of the $[\pm\theta]_s$ angle ply laminate cannot be directly linked to the longitudinal failure of each layer. Therefore, it is important to suppress those undesirable failure modes so the first mode of failure is longitudinal fibre failure in the plies.

It has been previously shown that by use of thin-plies, it is possible to suppress free-edge delamination and matrix cracking in angle-ply laminates under tension [12–14]. The energy release rate (G) at the free-edges of an angle-ply laminate is proportional to the thickness of each ply block [15] and use of plies with thickness of about 30 μm has been proved to successfully suppress any edge delamination. The effect of ply thickness on matrix cracking, known as 'in-situ' effect has been also well studied and it is known that reducing ply thickness leads to enhanced transverse strength and delayed matrix cracking [16]. Therefore, both free-edge delamination and matrix cracking can be avoided if the $[\pm\theta]_s$ angle-ply laminate is made from thin-ply blocks.

As previously shown by the authors [5], the end-tab stress concentration can be completely eliminated by embedding the laminate of interest ($[\pm\theta]_s$ angle-ply carbon laminate in this study) in between unidirectional glass layers. Including the glass layers on either side of the tested laminate means that the stress in the $[\pm\theta]_s$ angle-ply carbon laminate at failure cannot be directly calculated from the testing machine loadcell outputs but since the strain is uniform across the thickness, in-plane strain can be directly measured using any conventional extension measurement technique.

Since the fibre direction stress, σ_1, and the magnitude of in-plane shear stress, τ_{12} are equal in all individual carbon layers of the $[\pm\theta]_s$ angle-ply carbon laminate, no fibre failure strain enhancement is expected to occur due to the use of thin-plies and only the free-edge delamination and matrix cracking are expected to be suppressed. This is because the thickness of the $[\pm\theta]_s$ angle-ply carbon laminate is about 120 μm, very close to the thickness of a standard ply carbon layer.

Another important benefit of having glass layers on the outer layers is the visualisation of damage in the CFRP angle-ply laminate, as soon as it happens and starts to delaminate from the glass layers [17,18]. This means that identifying the damage and where it initiates from is simpler with the use of glass layers on the outer layers.

Fig. 2 shows a schematic of the final configuration for manufacturing and testing, a $[0_G/\pm\theta_C]_s$ layup, where G and C stands for glass and carbon layer respectively and the carbon layers will be thin-ply. The details of finding suitable θ values and thickness of each glass and carbon sub-laminate are discussed in the next section.
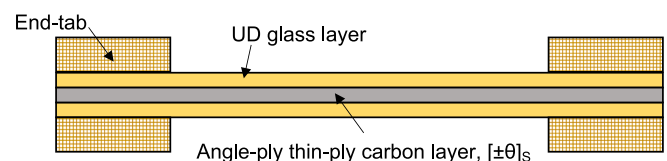

Fig. 2. Side view schematic of the angle-ply thin-ply carbon laminate embedded in glass layers.

3. Layup and specimen design

To cover a wide range of tension-shear combinations, six different sets of $[0_G/\pm\theta_C]_s$ samples with θ = 0°, 5°, 10°, 15°, 20° or 25° is studied. SkyFlex USN020 carbon/epoxy manufactured by SK Chemicals is selected as the tested carbon laminae based on several years of the group's experience on handling it and previous characterisation including the paper [19] to study the effect of carbon sub-laminate thickness on the fibre failure strain and hybrid effect. This paper [19] showed that CFRP sub-laminates with one and two 30 μm thin-ply carbon layers embedded in glass layers have enhanced failure strains when compared to thicker CFRP laminates with minimum thickness of around one standard ply, 125 μm. This means that to avoid any enhanced fibre failure strain, at least four thin-plies in the CFRP angle-ply sub-laminate are required. E-glass/913 epoxy manufactured by Hexcel was used as the 0° translucent glass layer on either side of the angle-ply carbon laminate. Table 1 shows the elastic in-plane properties, cured nominal thickness and fibre mass per unit area of each of the used materials. It is worth mentioning that SK Chemicals has used different types of carbon fibres in their USN020A prepreg products. The carbon fibre in our batch was TAIRYFIL TC-35 with failure strain of 1.7 % for 3 k and 6 k bundles and 1.8 % for 12 k, 24 k and 48 k according to the fibre manufacturer datasheet [20].

To be able to find the suitable thickness of each of the unidirectional glass and angle-ply carbon sub-laminates, the damage mode map technique [21,22] developed for achieving the desired failure process in hybrid composites is used. Hybrid composites are typically made out of two fibre types with different failure strain. The fibre with lower failure strain is typically referred to as the Low Strain Material (LSM) and the other one with higher failure strain is addressed as High Strain Material (HSM)[23]. The damage mode map has four regions of (1) premature HSM failure, (2) LSM layer failure followed by unstable delamination, (3) LSM layer fragmentation and (4) LSM layer fragmentation followed by dispersed delamination. The horizontal axis of the map represents the relative thickness of the LSM and the vertical axis represents the absolute thickness of the LSM. These four regions are numbered in Fig. 3 (a) and further details of how to draw these maps and how to interpret them can be found in [21,22]. In this study, the angle-ply carbon laminate is the LSM and the UD glass layer is the HSM. The aim of our test layup design is to achieve a single crack in the angle-ply carbon laminate as our LSM therefore, the region of interest on the damage mode map is region (2) and the layups should be desined to sit in this region.

The damage mode map depends on the mechanical properties of both the low strain and high strain materials. The six angle-ply carbon laminates have different engineering Young's modulus E_x and failure strain $\hat{\varepsilon}_x$. Therefore, six different maps are plotted in Fig. 3. Classical Laminate Theory is used to estimate the loading direction engineering modulus of the $[\pm\theta_C]_s$ angle-ply laminates: E_x = 101.7 GPa, 99.7 GPa, 93.1 GPa, 86.7 GPa, 63.1 GPa and 44.3 GPa for θ = 0°, 5°, 10°, 15°, 20° and 25° respectively. Based on the manufacturer's datasheet [20] for small 3 k and 6 k bundles of fibres, the failure strain of the TC-35 carbon fibres used in the USN020A prepregs is assumed to be 1.7 %. Assuming that shear has no effect on the failure strain of the laminae, the loading direction failure strain of the angle-ply laminates ($\hat{\varepsilon}_x$) is estimated based on when the strain in the fibre direction, $\hat{\varepsilon}_1$, reaches 1.7 % as the fibre failure strain of the unidirectional material: $\hat{\varepsilon}_x$=1.7 %, 1.72 %, 1.77 %, 1.87 %, 2.04 % and 2.31 % for θ = 0°, 5°, 10°, 15°, 20° and 25° respectively. The E-glass layer failure strain is assumed to be 3.5 % for

the reference volume of 1 mm^3 with the elastic Young's modulus of 38.7 GPa as explained in [24].

On each map in Fig. 3, the location of two scaled layups of $[0_{2G}/\pm\theta_C]_s$ and $[0_{4G}/(\pm\theta)_{2C}]_s$, θ = 0°, 5°, 10°, 15°, 20° or 25° is shown. In all cases, both layups are in the region (2), single crack in the angle-ply carbon laminate as the LSM followed by unstable delamination, except θ = 25° where the $[0_{2G}/\pm25_C]_s$ is at the border of regions (2) and (4). Therefore, for θ = 0°, 5°, 10°, 15° and 20°, the thinner layup was selected for the experiments. For θ = 25°, both $[0_{2G}/\pm25_C]_s$ and $[0_{4G}/(\pm25)_{2C}]$ layups were selected for manufacturing and testing.

The combination of in-plane shear and transverse stresses (τ_{12} and σ_2) in the local material coordinate system of a carbon ply at the fibre failure point (σ_1 = 1729 MPa) for all the selected layups are listed in Table 2 and compared in Fig. 4. These values are found using Classical Laminate Theory. The values of transverse stresses are negligible and stay significantly lower than the shear stresses in all layups. This shows that the desired combined in-plane tension-shear stress is achieved.

The last column of Classical Laminate Theory results in Table 2 indicates the fibre strain in the glass layer, at carbon fibre strains equal to 1.7 %. The maximum normal strain in the glass layer is 2.31 % for the layups with θ = 25° which is relatively high for E-glass/913 glass layer but still is below the reference failure strain.

A linear elastic Finite Element model is used to study the effect of free-edges on the fibre and transverse direction stresses, σ_1 and τ_{12}. 8-node linear brick elements with reduced integration and hourglass control were used. The element size was 10 μm along the width direction at the free-edges and then gradually increased to reduce the number of elements. In the thickness direction, each thin-ply was meshed with two elements per layer, resulting in 15-μm elements and each glass layer was modelled with three elements. In the length direction, uniform element size of 100 μm were used in the loading direction. All nodes on one end of the sample were constrained in the loading direction and a uniform displacement was applied in the other end of the sample to represent tensile load applied to the sample.

Fig. 5 shows the fibre and transverse direction stresses, σ_1 and τ_{12} in the middle of the two $-\theta$ carbon layers at the mid-plane of the layup within the 1.0 mm at the free-edge for an applied strain of ε_x = 1.7%. From the 16 mm full width of the sample, the stress deviation from the values in the middle of the sample is limited to only about 0.2 mm around the edges.

The stresses around the free-edges are not constant due to the singularity at those edges and the termination of the fibres. If the fibre fracture initiates from those areas near the free-edges, this can jeopardise the efficacy of the proposed method for measuring the effect of shear stresses on fibre direction tensile strength. However, this is deemed an unlikely case. It will be explained in the presentation of experimental results that the obtained failure strains are the same for the UD, small off-axis angle specimens and close to the failure strains from large off-axis angle specimens. This suggests that the significant variation of stresses at the free-edges has not affected the failure strain along the fibre direction. Also, the significant reduction of the fibre direction stresses at the free-edges suggest lower probability of fibre failure initiation from those free-edges. If the damage initiated from the areas near the free-edges instead due to higher shear stresses, the experimental results would show sensitivity to the magnitude of these stresses. So, the samples with higher off-axis angle would fail at lower strains compared to those samples with lower off-axis angles, as the laminates

Table 1

Properties of the prepregs used in this study – Moduli and Poisson's ratios from [24] and thermal expansion coefficients from [29].

Prepreg type	Cured nominal thickness (mm)	Fibre mass per unit area (g/m2)	E1 [GPa]	E2 [GPa]	G12 [GPa]	v 12	α_1[1/K]	α_2[1/K]
Hexcel E–glass/913	0.125	192	38.7	15.4	4.3	0.3	2×10^{-6}	3×10^{-5}
SK Chemicals USN020A	0.030	20	101.7	6.0	2.4	0.3	-1×10^{-6}	4×10^{-5}
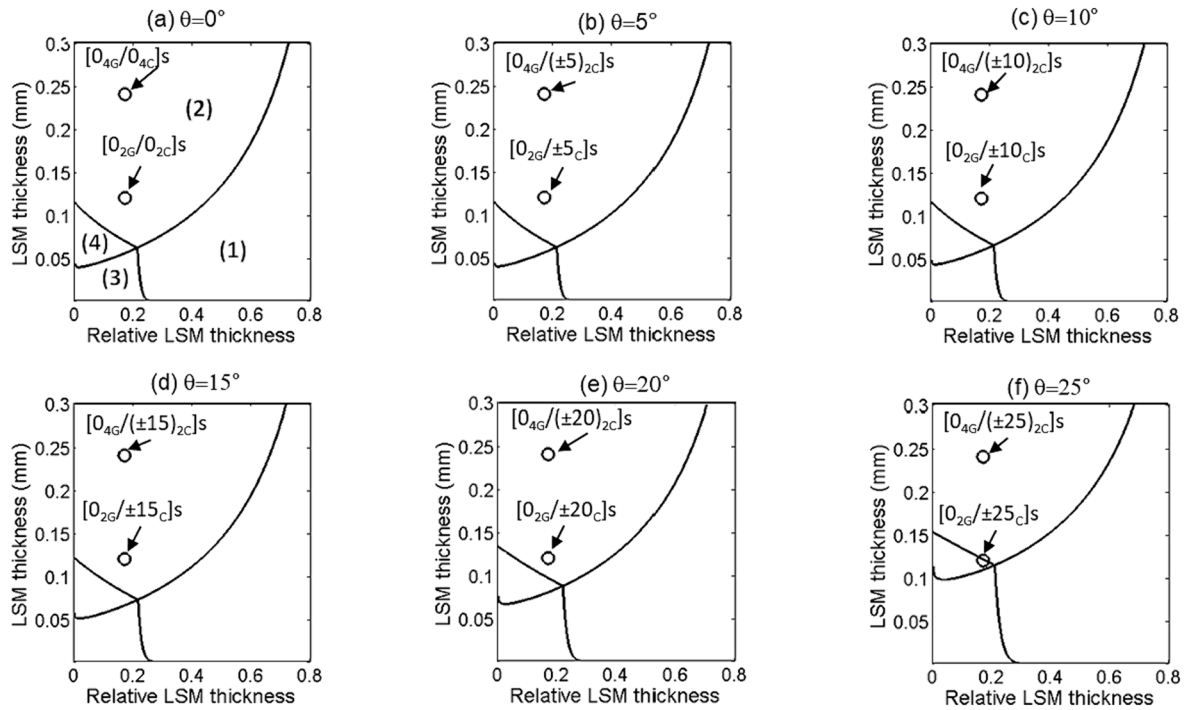
Fig. 3. (a-f) - Damage mode map for $[0_G/\pm\theta_C]_s$ layups with $\theta = 0°$, $5°$, $10°$, $15°$, $20°$ and $25°$.

Table 2
In-plane shear and transverse strain and stresses in the material coordinate system of a carbon ply and fibre direction strain in the glass layer at carbon fibres strain of 1.7%.

Layup	Classical Laminate Theory results						Finite Element results away the free-edges	
	Carbon layer local stress and strain					Glass layer strain	Carbon layer local stress	
	In-plane shear strain γ_{12} [%] at ε_1=1.7%	In-plane shear stress τ_{12} [MPa] at σ_1=1729 MPa	Normal transverse strain ε_2 [%] at σ_1=1729 MPa	Normal transverse stress σ_2 [MPa] at σ_1=1729 MPa	Strains due to curing residual stresses in fibre direction [%]	ε_{1G} [%] at ε_1=1.7%	In-plane shear stress τ_{12} [MPa] at σ_1=1729 MPa	Normal transverse stress σ_2 [MPa] at σ_1=1729 MPa
$[0_{2EG}/0_{2C}]_s$	0.00	0	-0.51	0	-0.0088	1.70%	0.00	0.00
$[0_{2EG}/\pm5_C]_s$	0.39	9.37	-0.51	-0.29	-0.0105	1.72%	9.37	-0.30
$[0_{2EG}/\pm10_C]_s$	0.56	19.46	-0.51	-1.02	-0.0156	1.77%	19.46	-1.02
$[0_{2EG}/\pm15_C]_s$	1.29	31.02	-0.49	-1.64	-0.0243	1.87%	31.01	-1.64
$[0_{2EG}/\pm20_C]_s$	1.87	44.93	-0.44	-1.23	-0.0364	2.04%	44.93	-1.23
$[0_{2EG}/(\pm25)_C]_s$ and $[0_{4EG}/(\pm25)_{2C}]_s$	2.60	62.34	-0.35	1.78	-0.0517	2.31%	62.34	1.79

with high off-axis angles have larger shear stress at the free-edges. As will be discussed, the experimental results have not shown this, and therefore, the fibre fractures are initiating from areas with constant stresses away from the free-edges.

Therefore, the free-edges are deemed not to alter or affect fibre failure in the carbon layers. In other words, the fibre failure in the carbon plies is only likely to start from points inside the laminates and therefore the proposed approach provides valid results.

Additionally, the experimental measured strain along the loading and transverse directions will not be affected by the free-edges as the area where the stresses deviate from the average stresses is only about 0.2 mm from the free edges,. Therefore, if the strains are measured experimentally away from the free-edges, they represent the average strains in the sample.

At points with more than 0.2 mm distance from the free-edges, the in-plane shear stress τ_{12} and normal transverse stress σ_2 are constant
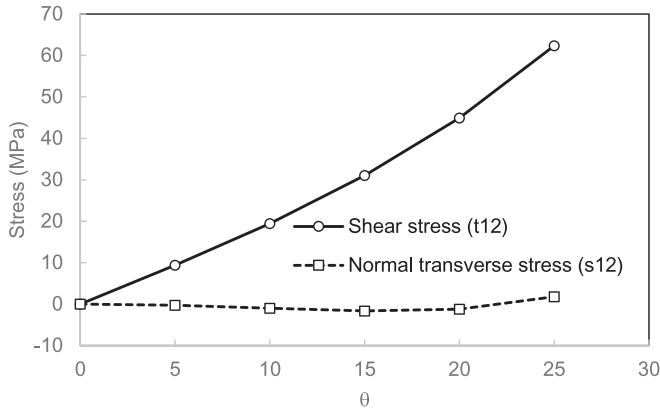
Fig. 4. Comparison of the in-plane shear and transverse stresses (τ_{12} and σ_2) in the local material coordinate system of $\theta°$ carbon ply at the carbon fibre failure point ($\sigma_1 = 1729$ MPa).

across the samples width and these stress values, found using FE at fibre direction stress of $\sigma_1 = 1729$ MPa in the carbon layers, are provided in the last two columns Table 2 and they match the analytical predictions in the same table, verifying the analytical results used in the design stage.

The strains caused by residual stresses due to the curing cycle are also calculated using Classical Laminate Theory and the values found to be small. The coefficient of thermal expansion of each material is provided in Table 1. Fibre direction residual elastic strains due to curing are provided in Table 2. The residual strain for $[0_{2EG}/(\pm25)_C]_s$ and $[0_{4EG}/(\pm25)_{2C}]_s$ layups is the largest value among all layups and is equal to only -0.0517 %. This is significantly smaller than the 1.7 % fibre failure strain and therefore, the residual strains are deemed not to likely affect the experimental results significantly.

The strain energy release rate values for delamination between θ and $-\theta$ layers, $\theta = 0°$, $5°$, $10°$, $15°$, $20°$, $25°$, at the free-edges of the chosen laminates at the predicted loading direction failure strain of $\hat{\varepsilon}_x = 1.7$ %, 1.72 %, 1.77 %, 1.87 %, 2.04 % and 2.31 % have been calculated to be equal to G = 0.000, 0.207, 0.503, 0.705, 0.847 and 0.960 N/mm using the method proposed in [25] and used extensively in [15]. It has been shown that for such angle-ply layup, the fracture is pure mode-II and therefore, the energy release rates should be compared against G_{IIc} of the material, which is estimated to be equal to 1.08 N.mm [15]. This shows that in none of the proposed laminates, we expect to have free-edge delamination as the energy release rate is below the fracture

toughness. This is due to use of thin-plies. The same analysis on hypothetical $[0_{2EG}/(\pm25)_C]_s$ laminates with standard carbon ply thickness of 0.125 mm gave an energy release rate of 4.510 N/mm, which is much higher than the fracture toughness of the material, indicating that standard-thickness carbon plies would lead to free-edge delamination before fibre failure. Since, thin carbon-plies of 0.030 mm thickness have been used in this work, there is no risk of free-edge delamination, and this is confirmed by the experimental results.

4. Experiments

4.1. Manufacture

Individual 300 mm by 300 mm squares of glass and carbon prepregs were cut using an automated cutting machine and stacked up to build the proposed layups. The composite laminates were cured in an autoclave with a two-step cure cycle of 60 min at 80 °C followed by 100 min at 125 °C under a constant 0.7 MPa pressure following the Hexcel 913 resin curing cycle. This curing cycle has previously been used for co-curing similar combinations of materials. The resins were found to be compatible, and the glass and carbon layers bonded well together. The plates were then cut into 270 mm long by 16 mm wide coupon size samples using a diamond-cutting wheel. End tabs of 16 mm width, 2 mm thickness and 40 mm length made out of woven glass/epoxy plates were attached to the laminates using a two-part Araldite 2000 adhesive. The final gauge length of the tensile samples was 190 mm. To ensure best adhesion performance, the end-tabbed samples were cured for 120 min at 80 °C in an oven.

4.2. Testing procedure

Tensile testing was done using a 25 kN computer controlled Instron 8892 hydraulic test machine. Crosshead speed was set at 2 mm/min with a grip pressure of 6.2 MPa. Vertical and horizontal strains on the specimens were measured using an Imetrum video gauge system. White dots were marked on a black paint at the top, bottom and sides in the middle section of each specimen to allow the system to track their relative positions (see Fig. 6). Videos of the failure process of each specimen were also taken to study the damage evolution. At least five specimens were tested for each lay-up configuration to ensure repeatability.

Initiation of internal damage was also determined by collecting acoustic emission data using the Mistras AE data acquisition system (PAC) PCI-2. The sensor was a R15 resonant-type, single-crystal piezo-electric transducer with 20–900 kHz frequency range. Two sensors, 55 mm from each end of the specimen, were attached using plastic clips.
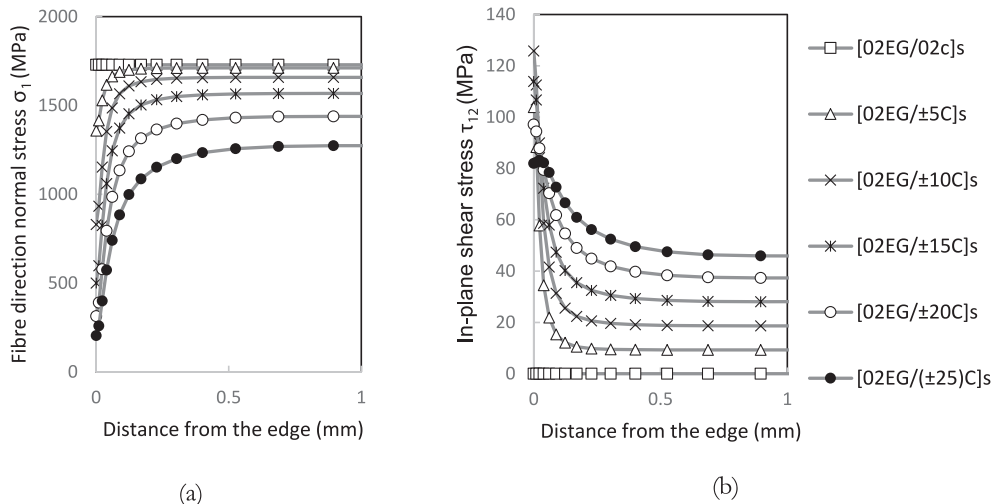

(a)

(b)

Fig. 5. Stress in the (a) fibre direction σ_1, (b) transverse shear direction, τ_{12}, within the $-\theta$ carbon layer near the free-edges of the sample from the FE analysis.
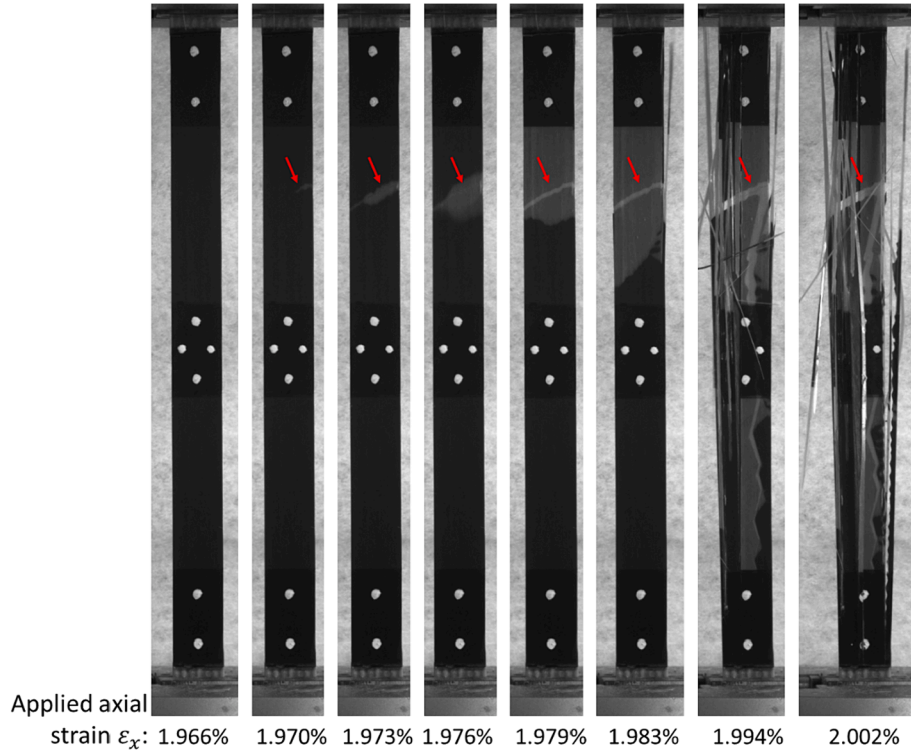
Fig. 6. Damage development of the $[0_{2EG}/\pm15_C]_s$ layup in the gauge section and far away from the end-tabs with visible change of appearance – Red arrow highlights the failure point in the $[\pm15_C]_s$ CFRP laminate.

The system was set to a sampling rate of 5 MHz with 60 dB minimum threshold.

4.3. Transformation of strains

The fibre direction strain, ε_1, and the shear strain in the local material coordinate system, γ_{12}, in the carbon layers for each layup are found using the experimentally measured ε_x and ε_y using the strain transformation relationships below.

$$\varepsilon_1 = \frac{\varepsilon_x + \varepsilon_y}{2} + \frac{\varepsilon_x - \varepsilon_y}{2}\cos2\theta + \frac{\gamma_{xy}}{2}\sin2\theta$$

$$\frac{\gamma_{12}}{2} = -\frac{(\varepsilon_x - \varepsilon_y)}{2}\sin2\theta + \frac{\gamma_{xy}}{2}\cos2\theta \qquad (1)$$

Where the shear strain in the loading direction coordinate system is zero, $\gamma_{xy}=0$ and is omitted from the equations.

5. Experimental results

Fig. 6 shows the development of damage in one of the $[0_{2EG}/\pm15_C]_s$ samples provided as an example. The first damage mode is a single crack in the $[\pm15_C]_s$ carbon laminate developed catastrophically across the width in the gauge section. This single crack has been highlighted with a red arrow in Fig. 6 and there is no damage prior to this in the laminate. This is then followed by delamination between the glass and carbon laminates and finally, the glass layers fail due to fibre failure. Fig. 7 (a) shows the stress–strain curves of five different $[0_{2EG}/\pm15_C]_s$ specimens up to their failure point. All the samples have a linear elastic behaviour
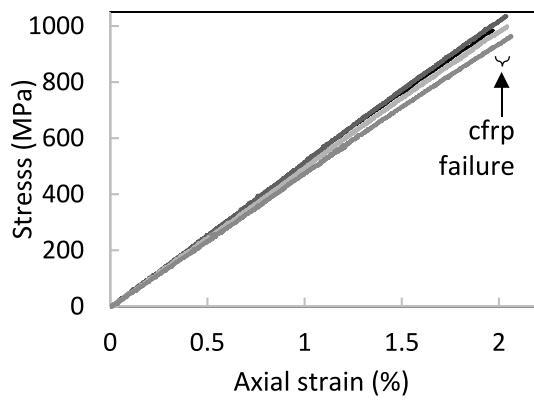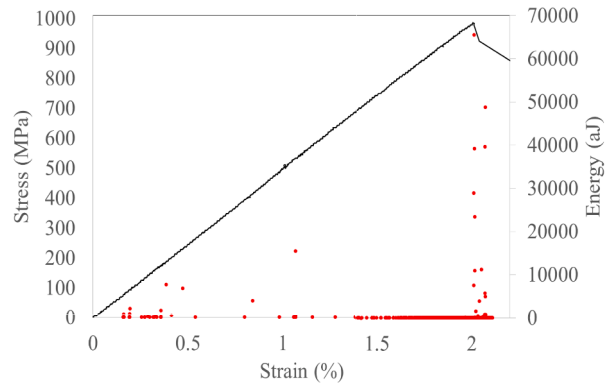
Fig. 7. (a) Stress–strain curves of five different $[0_{2EG}/\pm15_C]_s$ specimens with linear-elastic behaviour (b) Acoustic emission results versus stress–strain curve of a $[0_{2EG}/\pm15_C]_s$ sample.

and the scatter in the measured final failure strain is very small. Fig. 7 (b) shows the acoustic emission results for the $[0_{2EG}/\pm15_C]_s$ sample, indicating that up to the final failure point, there was a negligible number of acoustic energy signals recorded. These acoustic energy signals are not due to matrix cracking or delamination at the free-edge due to the low number of incidents and are believed to be due to superficial testing limitations, e.g. separation of mis-aligned fibres from the edge of the samples. This indicates that the crack in the carbon laminate shown in Fig. 6 was indeed the first major mode of failure in this layup.

Fig. 8 shows different samples with different layups and carbon fibre orientation after their final failure. A single crack in the carbon laminate, far away from any end-tab is a clear indication that the desired failure process has been achieved in all tested samples. The acoustic emission recordings of these samples indicate no significant damage e.g. free-edge delamination or matrix cracking before the single crack in the carbon sub-laminate. The stress–strain curves of all these samples were linear elastic and similar to the $[0_{2EG}/\pm15_C]_s$ layup shown in Fig. 7 (a) and therefore are not provided.

Table 3 includes the average results for all of the tested samples. The first column is the average failure stress $(\hat{\sigma}_x)$ applied to the samples calculated by dividing the failure force by the measured total cross-section of each sample. The Coefficients of Variation (CV) of the results are also included in brackets below the average value. The next two columns are the average failure strain in the vertical loading and horizontal y direction strains $(\hat{\varepsilon}_x$ and $\hat{\varepsilon}_y)$ measured using the video gauges. The obtained loading direction strain at the failure point, $\hat{\varepsilon}_x$, gradually increases at larger θ values and this is in agreement with the trend in Table 2, in which, the glass fibre strains at failure increased due to the increase in the off-axis θ angle of the carbon layers. The coefficients of variation of the $\hat{\varepsilon}_x$ values are between 1.1 % and 4.4 %, indicating the repeatability and low scatter in the results. The coefficients of variation of the $\hat{\varepsilon}_y$ values are slightly higher, mostly below 10 %, and are still acceptable. Using Eq. (1) as well as the measured $\hat{\varepsilon}_x$ and $\hat{\varepsilon}_y$ values in Table 3, the fibre, transverse and shear strains at the failure point in the local material coordinate system, $\hat{\varepsilon}_1$, $\hat{\varepsilon}_2$ and $\hat{\gamma}_{12}$, are calculated and the average values are shown in Table 3. The final column in this table is the sum of the fibre direction strain due to mechanical loading and the residual strain calculated from Classical Laminate Theory to find the fibre

direction strain corrected for the residual strains due to curing. The residual strains are all small and the corrected value is not significantly changed.

The coefficients of variation of $\hat{\varepsilon}_1$ are all below 5 % and for the $\hat{\gamma}_{12}$ values, the coefficients of variation are all below 6.1 % except the $[0_{2EG}/(\pm25)_C]_s$ layup with a coefficient of variation of 7.1 %. Overall, the scatter in the results is small and the tests were repeatable. Fig. 9 (a) indicates the fibre failure strains against shear strains of all tested samples individually. Since the scatter in the shear strains of the $[0_{2EG}/(\pm25)_C]_s$ layup was slightly higher than the other laminates, and since the location of this layup on the damage mode map in Fig. 3 (e) was too close to the boundary of region 4, the results of this layup are shown using a cross marker (×) and all other specimens are indicated by a circle. The dashed line joins the averages of the fibre failure strain and shear strain values of all five samples in each layup configuration excluding those of the $[0_{2EG}/(\pm25)_C]_s$ case.

The presence of shear strain, even with high values, has not significantly changed the carbon layer longitudinal failure strain and the reduction in the failure strain is quite small compared to the traditional combined stresses criteria e.g. Tsai-Hill.

6. Discussion

Fig. 9 (b) shows the error bars of the fibre direction and shear strains at failure of the CFRP sub-laminates. The obtained experimental results have a small scatter proving that the proposed method provides repeatable test results. This repeatability was observed in almost all aspects of the results, from measured failure strains in the loading coordinate system $(\hat{\varepsilon}_x$ and $\hat{\varepsilon}_y)$ to the processed longitudinal and shear final failure strains in the local carbon ply coordinate system $(\hat{\varepsilon}_1$ and $\hat{\gamma}_{12})$. This is very positive when we consider the concerns shared in WWFE [1] about lack of reliable experimental results.

As mentioned earlier, two values of fibre failure strains of 1.7 % and 1.8 % were mentioned in the TC-35 datasheet [20] for small and bigger fibre bundles. At the design stage, we assumed the failure strain of USN020 to be equal to 1.7 % but the obtained results in Table 3 show that the failure strain of this prepreg layer is around at least 1.8 %. The vertical line of $\hat{\varepsilon}_1 = 1.8\%$ in Fig. 9(b) passes through the error bands for


$[0_{2EG}/0_{2C}]_s$ $[0_{2EG}/\pm5_C]_s$ $[0_{2EG}/\pm10_C]_s$ $[0_{2EG}/\pm15_C]_s$ $[0_{2EG}/\pm20_C]_s$ $[0_{2EG}/(\pm25)_C]_s$ $[0_{4EG}/(\pm25)_{2C}]_s$

Fig. 8. Samples with different fibre orientations of q = 0°, 5°, 10°, 15°, 20°, 25° (8 plies and 16 plies) after final failure indicating crack in the carbon layer occurring far away from the end-tabs.

Table 3
Summary of the obtained results including the measured strain values and calculated fibre direction and shear strain values at the failure of the carbon angle-plies.

Layup	Failure stress $\widehat{\sigma}_x$ [MPa] (CV [%])	Failure strain $\widehat{\varepsilon}_x$ [%] (CV [%])	Failure strain $\widehat{\varepsilon}_y$ [%] (CV[%])	longitudinal failure strain $\widehat{\varepsilon}_1$ [%] (CV [%])	Transverse strain $\widehat{\varepsilon}_2$ [%] (CV[%])	Shear strain $\widehat{\gamma}_{12}$ [%] (CV [%])	Corrected longitudinal failure strain $\widehat{\varepsilon}_1$ considering residual strains from CLT [%]
$[0_{2EG}/0_{2c}]_s$	978.6 (2.41)	1.834 (1.09)	−0.672 (13.17)	1.834 (1.09)	−0.672 (13.17)	0.000 (-)	1.8252
$[0_{2EG}/\pm5_C]_s$	987.8 (2.52)	1.872 (3.99)	−0.641 (4.48)	1.853 (3.99)	−0.622 (4.51)	0.436 (3.92)	1.8425
$[0_{2EG}/\pm10_C]_s$	969.2 (1.25)	1.874 (2.58)	−0.730 (7.41)	1.796 (2.55)	−0.651 (7.89)	0.891 (3.63)	1.7804
$[0_{2EG}/\pm15_C]_s$	993.4 (2.66)	2.022 (1.76)	−0.828 (6.67)	1.831 (1.76)	−0.637 (7.98)	1.425 (2.59)	1.8067
$[0_{2EG}/\pm20_C]_s$	983.8 (6.82)	2.120 (4.37)	−0.951 (6.42)	1.761 (4.53)	−0.592 (8.66)	1.974 (4.14)	1.7246
$[0_{4EG}/(\pm25)_{2C}]_s$	1023.8 (5.10)	2.329 (3.36)	−1.230 (5.08)	1.693 (3.52)	−0.594 (7.77)	2.726 (3.42)	1.6413
$[0_{2EG}/(\pm25)_C]_s$	992.6 (4.91)	2.244 (4.41)	−1.097 (10.30)	1.647 (3.75)	−0.500 (15.12)	2.559 (6.31)	1.5953
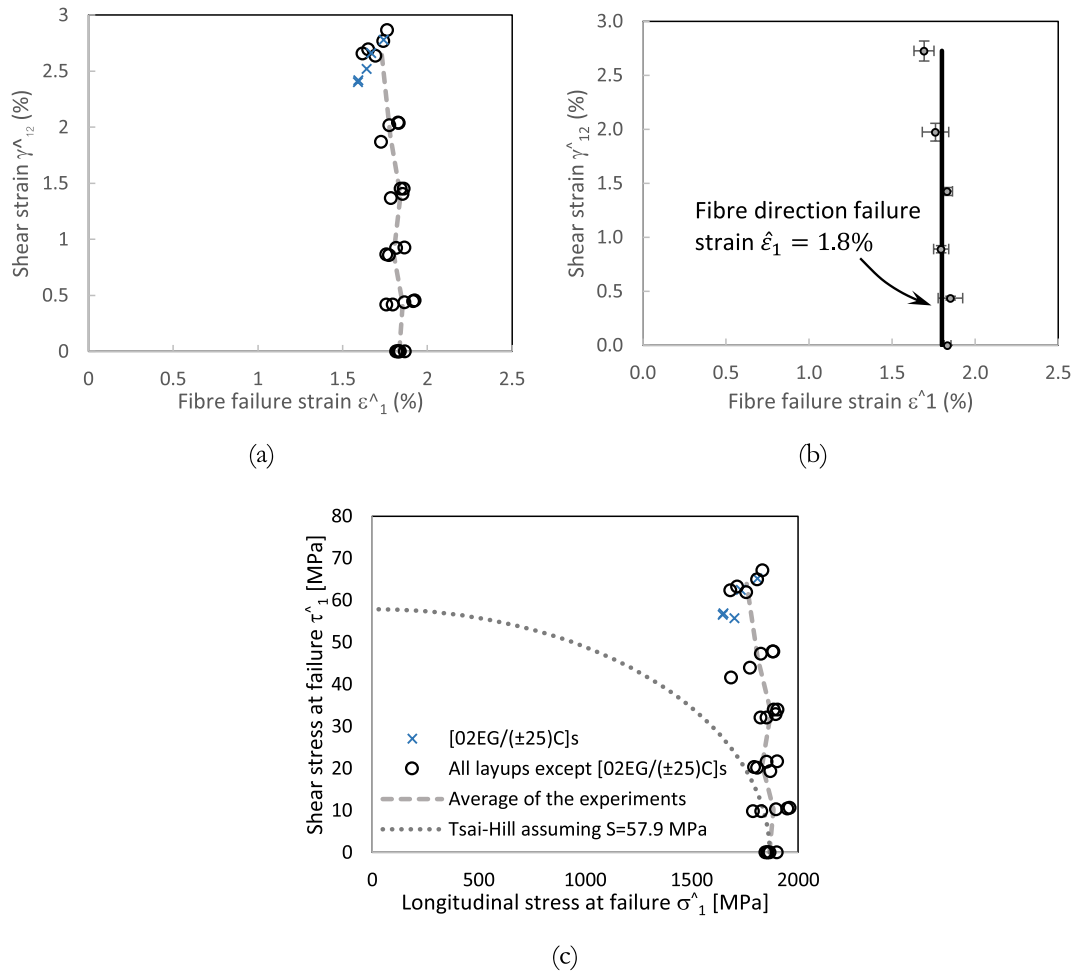
Fig. 9. (a) The failure line for fibre direction tensile and in-plane shear combined stress state, (b) Fibre direction tensile and in-plane shear strain error bars against fibre direction strain of $\widehat{\varepsilon}_1 = 1.8\%$, (c) Fibre direction and shear failure stresses assuming a linear-elastic response.

all points except the point with the highest shear strain of 2.7 % and it is still quite close to that point too.

The obtained experimental results show that there is no significant reduction of tensile longitudinal failure strains of carbon plies when exposed to up to 2.0 % in-plane shear strains and only a small 6 % reduction in longitudinal failure strain at 2.7 % in-plane shear strain. This suggests that interactive models in which, the presence of shear stress results in prediction of lower tensile failure stress, are not applicable to the carbon fibre epoxy laminate tested in this study. A similar experimental campaign could be done on other composite materials.

Fig. 9 (c) shows the obtained experimental fibre direction failure stresses against their shear stresses, assuming that the material has a linear elastic response. Also, the Tsai-Hill interactive criterion is plotted

for the shear strength of the carbon plies equal to 57.9 MPa based on ASTM D3518 standard in [26]. Clearly, the interactive model is not matching the experimental results. While the shear stresses of the experimental points on Fig. 9 (c) are not necessarily precise, as composites are known to have a non-linear shear response, most of the interactive models e.g. Tsai-Hill used for this figure are applied based on linear-elastic analysis anyway. It is worth mentioning that the maximum shear stress in the carbon layers in ±45° shear was estimated to be 88 MPa in [27] based on the simple equation ignoring non-linearity. This is significantly higher than the value used to plot Fig. 9 (c), but is believed to be too high given the significant fibre rotation at the very high strain in this test and so the more realistic value of 57.9 MPa is used to draw Fig. 9 (c).

Additionally, in more standard carbon fibre composite laminates where there are typically combinations of 0°, 45° and 90° plies, the in-plane shear strains could not reach such high values. From a consideration of the strain transformation equations, a pure shear strain in the 0° direction will result in a direct strain of equal magnitude at 45°. Failure in the fibre direction would be expected to occur first in the 45° plies before such high shear strains as applied in the current study could be reached. Therefore, the authors' conclusion is that the fibre direction failure stress of the tested carbon material is not likely to be affected at all by in-plane shear stresses in realistic laminates. Similar studies on other carbon fibre materials and layups would be interesting to provide further insight and confirm the validity of this conclusion for a wider range of laminates.

The normal transverse strains, $\widehat{\varepsilon}_2$, in Table 3 follow a similar trend to ε_2 calculated from Classical Laminate Theory in Table 2. The values of ε_2 in Table 2 start at -0.51 % for $\theta = 0°$ and gradually change to -0.35 % for $\theta = 25°$. In the experimental results in Table 3, $\widehat{\varepsilon}_2$, values change gradually from -0.67 % to -0.59 % for the $[0_{4EG}/(\pm 25)_{2C}]_s$ layup. The values in Table 2 are calculated for 1.7 % fibre direction strain, $\varepsilon_1 = 1.7$ %, but those experimental results in Table 3 are occurring mostly at strains more than 1.8 %. At similar fibre direction strains, the transverse strain values, ε_2, would be closer. Also, the laminate calculations assumed linear material properties, whereas the shear and to some extent the transverse ply response is in fact non-linear.

The average failure strains from the $[0_{4EG}/(\pm 25)_{2C}]_s$ and $[0_{2EG}/(\pm 25)_C]_s$ layups are close, but the results from the $[0_{4EG}/(\pm 25)_{2C}]_s$ layup have less scatter and were used to draw the average line in Fig. 9 (a).

Curing off-axis and dis-similar materials causes residual stresses in the laminate. The residual strains in the fibre direction of the CFRP plies induced by the curing cycle have been calculated for all of the layups and are equal to -0.0088 %, -0.0105 %, -0.0156 %, -0.0243 %, -0.0364 % and -0.0517 % respectively for $\theta = 0°$, 5°, 10°, 15°, 20° or 25° as presented in Table 2. This shows that the residual strains are negligible and do not affect the conclusions above [28].

The use of thin plies in this method is one of the limitations. If the thin-plies used are simply replaced by standard plies, there is a risk of matrix cracking and delamination, especially around the free-edges. For standard ply thickness prepregs, the use of higher toughness matrices may alleviate this issue by suppressing the interlaminar damage and perhaps the matrix cracking. Further experimental work is required to study and understand the effect of thicker plies and tougher matrices on the wider applicability of the proposed technique.

It is worth mentioning that this work does not account for the potential increases or changes in scatter that would result from the manufacturing process of large components. Therefore, the results of the experimental method proposed here should not be used directly in determining design allowables of industrial components unless all sources of scatter which may be present in a final component are accounted for.

7. Conclusion

Overall, the objective of developing a new technique to investigate tensile fibre direction failure in the presence of in-plane shear stress whilst avoiding premature failure was achieved successfully with small scatter in the results. More specific conclusions are listed below.

- *The new method demonstrates negligible interaction between in-plane shear strains and the fibre failure strains of the tested carbon/epoxy laminate:* While some interactive failure criteria suggest that in-plane shear stress reduces the longitudinal failure stress, the authors did not observe any significant reduction of fibre direction failure strain at high shear strain conditions. In typical layups with 0°, 45° and 90° plies, fibre direction failure would be expected to occur in the 45° plies well before reaching the high levels of shear strains applied in

this study, suggesting that shear stresses are not likely to affect tensile failure in realistic laminates.
- *The manufacture of samples is significantly easier than other proposed techniques*: The samples in this method are flat specimens obtained following standard manufacturing techniques. They are significantly easier and cheaper to manufacture than tubular samples. The ease of manufacture reduces the chance of unwanted defects during the manufacturing process and allows more laboratories to be able to carry out such combined stress state tests.
- *Only application of tensile loading is required*: The only required external loading is a tensile load which is significantly easier and cheaper to apply compared with simultaneous tension and torsion loads on non-flat samples e.g. tubular specimens.
- *The obtained experimental results show smaller scatter than those from tubular specimens*: The method proved to be reliable and repeatable, providing results consistent with the material datasheet with co-efficients of variation of most results below 5 %. Tubular specimens typically have significantly larger coefficient of variation or fail prematurely. This improvement is due to simpler geometry, manufacturing, testing and elimination of end-tab stress concentrations.

Declaration of competing interest

The authors declare that they have no known competing financial interests or personal relationships that could have appeared to influence the work reported in this paper.

Data availability

No data was used for the research described in the article.

References

[1] Hinton MJ, Kaddour AS, Soden PD. A comparison of the predictive capabilities of current failure theories for composite laminates, judged against experimental evidence. Compos. Sci. Technol. 2002;62:1725–97. https://doi.org/10.1016/S0266-3538(02)00125-2.

[2] ISO - ISO 527-5:2009 - Plastics — Determination of tensile properties — Part 5: Test conditions for unidirectional fibre-reinforced plastic composites n.d. https://www.iso.org/standard/52991.html (accessed January 1, 2021).

[3] ASTM D5083 - 17 Standard Test Method for Tensile Properties of Reinforced Thermosetting Plastics Using Straight-Sided Specimens n.d. https://www.astm.org/Standards/D5083.htm (accessed January 1, 2021).

[4] ASTM D3039 / D3039M - 08 Standard Test Method for Tensile Properties of Polymer Matrix Composite Materials n.d. https://www.astm.org/DATABASE.CART/HISTORICAL/D3039D3039M-08.htm (accessed January 1, 2021).

[5] Czél G, Jalalvand M, Wisnom MR. Hybrid specimens eliminating stress concentrations in tensile and compressive testing of unidirectional composites. Compos. A Appl. Sci. Manuf. 2016. https://doi.org/10.1016/j.compositesa.2016.07.021.

[6] Chen AS, Matthews FL. A review of multiaxial/biaxial loading tests for composite materials. Composites 1993;24:395–406. https://doi.org/10.1016/0010-4361(93)90247-6.

[7] Thom H. A review of the biaxial strength of fibre-reinforced plastics. Compos. A Appl. Sci. Manuf. 1998;29:869–86. https://doi.org/10.1016/S1359-835X(97)00090-0.

[8] Soden PD, Hinton MJ, Kaddour AS. Biaxial test results for strength and deformation of a range of E-glass and carbon fibre reinforced composite laminates. failure exercise benchmark data. Fail Criteria Fibre-Reinforced-Polymer Compos 2004;62:52–96. https://doi.org/10.1016/B978-008044475-8/50004-4.

[9] Michaeli W, Mannigel M, Preller F. On the effect of shear stresses on the fibre failure behaviour in CFRP. Compos. Sci. Technol. 2009;69:1354–7. https://doi.org/10.1016/J.COMPSCITECH.2008.09.024.

[10] T300 Data Sheet, Toray Composite Materials America Inc. 2018.

[11] D 3039/D 3039M Standard Test Method for Tensile Properties of Polymer Matrix Composite Materials. vol. 15. 2002.

[12] Sihn S, Kim RY, Kawabe K, Tsai SW. Experimental studies of thin-ply laminated composites. Compos. Sci. Technol. 2007;67:996–1008. https://doi.org/10.1016/j.compscitech.2006.06.008.

[13] Fuller JD, Wisnom MR. Pseudo-ductility and damage suppression in thin ply CFRP angle-ply laminates. Compos. A Appl. Sci. Manuf. 2015;69:64–71. https://doi.org/10.1016/j.compositesa.2014.11.004.

[14] Fuller JD, Jalalvand M, Wisnom MR. Combining fibre rotation and fragmentation to achieve pseudo-ductile CFRP laminates. Compos. Struct. 2016;142. https://doi.org/10.1016/j.compstruct.2016.01.073.

[15] Ubago Torres M, Jalalvand M. Additive binding layers to suppress free edge delamination in composite laminates under tension. Compos. A Appl. Sci. Manuf. 2022;156:106902. https://doi.org/10.1016/j.compositesa.2022.106902.

[16] Camanho PP, Dávila CG, Pinho ST, Iannucci L, Robinson P. Prediction of in situ strengths and matrix cracking in composites under transverse tension and in-plane shear. Compos. A Appl. Sci. Manuf. 2006;37:165–76. https://doi.org/10.1016/J.COMPOSITESA.2005.04.023.

[17] Rev T, Jalalvand M, Fuller J, Wisnom MR, Czél G. A simple and robust approach for visual overload indication - UD thin-ply hybrid composite sensors. Compos. A Appl. Sci. Manuf. 2019;121. https://doi.org/10.1016/j.compositesa.2019.03.005.

[18] Fotouhi S, Jalalvand M, Wisnom MR, Fotouhi M. Smart hybrid composite sensor technology to enhance the detection of low energy impact damage in composite structures. Compos. A Appl. Sci. Manuf. 2023;172:107595. https://doi.org/10.1016/j.compositesa.2023.107595.

[19] Wisnom MR, Czél G, Swolfs Y, Jalalvand M, Gorbatikh L, Verpoest I. Hybrid effects in thin ply carbon/glass unidirectional laminates: accurate experimental determination and prediction. Compos. A Appl. Sci. Manuf. 2016;88. https://doi.org/10.1016/j.compositesa.2016.04.014.

[20] Formosa Plastics Group. TAIRYFIL Data Sheet Automotive 2017. https://www.formosam.com/wp-content/uploads/2019/06/型錄汽車用.pdf (accessed December 30, 2021).

[21] Jalalvand M, Czél G, Wisnom MR. Parametric study of failure mechanisms and optimal configurations of pseudo-ductile thin-ply UD hybrid composites. Compos. A Appl. Sci. Manuf. 2015;74. https://doi.org/10.1016/j.compositesa.2015.04.001.

[22] Jalalvand M, Czél G, Wisnom MRMR. Damage analysis of pseudo-ductile thin-ply UD hybrid composites - a new analytical method. Compos. A Appl. Sci. Manuf. 2015;69:83–93. https://doi.org/10.1016/j.compositesa.2014.11.006.

[23] Wisnom MR, Pimenta S, Shaffer MSP, Robinson P, Potter KD, Hamerton I, et al. High performance ductile and pseudo-ductile Polymer matrix composites: a review. Compos. A Appl. Sci. Manuf. 2024. https://doi.org/10.1016/j.compositesa.2024.108029.

[24] Jalalvand M, Czél G, Wisnom MR. Numerical modelling of the damage modes in UD thin carbon/glass hybrid laminates. Compos. Sci. Technol. 2014;94. https://doi.org/10.1016/j.compscitech.2014.01.013.

[25] O'brien TK.. Characterization of delamination onset and growth in a composite laminate. Damage Compos Mater ASTM STP 1982:140–67.

[26] Rev T. Exploiting thin-ply materials to establish controlled failure in carbon composites. University of Bristol; 2020. PhD thesis.

[27] Fuller JD, Wisnom MR. Pseudo-ductility and damage suppression in thin ply CFRP angle-ply laminates. Compos. A Appl. Sci. Manuf. 2014;69:64–71. https://doi.org/10.1016/j.compositesa.2014.11.004.

[28] Suwarta P. Pseudo-ductility of unidirectional thin-ply hybrid composites. University of Bristol; 2020. PhD Thesis.

[29] Rev T, Wisnom MR, Xu X, Czél G. The effect of transverse compressive stresses on tensile failure of carbon fibre/epoxy composites. Compos. A Appl. Sci. Manuf. 2022;156. https://doi.org/10.1016/j.compositesa.2022.106894.